Resolving leaf level metabolism of C_4 *Setaria viridis* acclimated to low light through a biochemical model

Chandra Bellasio[a, b*], Maria Ermakova[b]

[a] Department of Biology, University of the Balearic Islands, 07122 Palma, Illes Balears, Spain.
[b] Australian Research Council Centre of Excellence for Translational Photosynthesis, Division of Plant Science, Research School of Biology, The Australian National University, Acton, Australian Capital Territory 2601, Australia.
[*] Correspondence: Chandra Bellasio (chandra.bellasio@uib.es)

Abstract

When C_4 plants are exposed to low light, CO_2 concentration in the bundle sheath (BS) decreases, causing an increase in photorespiration, leakiness (the ratio of CO_2 leak rate out of the BS over the rate of supply via C_4 acid decarboxylation), and a consequent reduction in biochemical efficiency. This can to some extent be mitigated by complex acclimation syndromes, which are of primary importance for crop productivity, but not well studied. We unveil a strategy of leaf-level low light acclimation involving regulation of electron transport processes. Firstly, we characterise anatomy, gas-exchange and electron transport of *Setaria viridis* grown under low light. Through a newly developed biochemical model we resolve the photon fluxes, and reaction rates to explain how these concerted acclimation strategies sustain photosynthetic efficiency. Smaller BS in low light-grown plants limited leakiness but sacrificed light harvesting and ATP production. To counter ATP shortage and maintain high assimilation rates, plants facilitated light penetration through mesophyll and upregulated cyclic electron flow in the BS. This novel shade tolerance mechanism based on optimisation of light reactions is more efficient than the known mechanisms involving the rearrangement of dark reactions and can potentially lead to innovative strategies for crop improvement.

Keywords:

C_4 photosynthesis, Kranz anatomy, light harvesting, bundle sheath, cyclic electron flow, gas-exchange, modelling

Significance

We mechanistically link the optical cross section with the rate of electron transport, the engagement of cyclic electron flow, the relative rate of ATP and NADPH generation, and ultimately the apportioning of dark reactions between mesophyll and bundle sheath cells. The striking capacity of *S. viridis* to acclimate light reactions presents a novel and perhaps the most

efficient shade tolerance strategy, potentially leading to novel possibilities for crop improvement.

Introduction

Leaves of the majority of C_4 plants are organised in two concentric cylinders (Figure 1). Mesophyll (M) cells surrounded by intercellular airspace radiate from bundle sheath (BS) cells, adjacent to the vasculature. CO_2 entering the leaves is first hydrated to HCO_3^- by carbonic anhydrase (CA) in the cytosol of M cells, and then fixed by PEP carboxylase (PEPC) into C_4 acids, which may be transaminated or chemically reduced (Figure 2). C_4 (amino)acids diffuse to BS cells where they are decarboxylated either primarily by NADP-malic enzyme (NADP-ME), NAD-malic enzyme (NAD-ME), PEP carboxykinase (PEPCK), or by a combination of them. Decarboxylation provides higher CO_2 partial pressure at the site of ribulose bisphosphate carboxylase oxygenase (Rubisco; for this function C_4 photosynthesis is also referred to as biochemical CO_2 concentrating mechanism, CCM) thereby largely suppressing the competitive reaction with oxygen leading to the wasteful process of photorespiration (von Caemmerer and Furbank, 2003, Bellasio *et al.*, 2014). Pyruvate resulting from the C_4 acids decarboxylation diffuses back to M cells where it is regenerated into PEP by pyruvate ortophosphate dikinase (PPDK) using 2 ATP molecules. Some of the CO_2 released in BS cells diffuses out to M cells (called leakage) and the refixation of that escaping CO_2 incur in an additional ATP cost of C_4 photosynthesis (Farquhar, 1983, Henderson *et al.*, 1992, Bellasio and Griffiths, 2014a).

C_4 photosynthesis is highly sensitive to limiting light intensities. Under low irradiance, ATP generation slows down, limiting the regeneration of PEP, and the activity of PEPC (V_P), mediated by light-regulation (Bailey *et al.*, 2007). This lowers the rate of C_4 acids export to the BS, their decarboxylation, and, as a result, reduces the CO_2 concentration in BS cells (C_{BS}). Consequently, the relative photorespiration rate increases and the overall biochemical operating efficiency of C_4 photosynthesis, quantified as ATP demand for gross assimilation, decreases (Furbank *et al.*, 1990, Ubierna *et al.*, 2013). In crop canopies where up to 50 % of net CO_2 uptake is fixed by shaded leaves (Baker *et al.*, 1988, Long, 1993) light limitations play an important role in decreasing canopy productivity (Kromdijk *et al.*, 2010), and understanding acclimation strategies of C_4 metabolism to light limitations is critical for crop production (Evans *et al.*, 1991, Bellasio and Griffiths, 2014a).

To meet the NADPH and ATP demands of each cell type, incident light is effectively shared between the electron transfer chains of M and BS cells (Kramer and Evans, 2011). ATP may be produced in the BS (mainly through cyclic electron flow, CEF, around Photosystem I, PSI)

or in the M (mainly through linear electron flow, LEF) depending on the light locally available in BS or M. In this way, the apportioning of excitation energy between the two cell types will influence the availability of ATP and NADPH in the BS or in the M (Bellasio and Griffiths, 2014c). For instance, green light is not strongly adsorbed by mesophyll cells and can preferentially excite bundle sheath cells, or v*ice versa* for blue light (Evans *et al.*, 2007). Because bundle sheaths are surrounded by mesophyll, light harvesting in the M will reduce the light available to reach BS cells (Bellasio and Lundgren, 2016). Also, the BS optical cross section and the BS size limit the amount of light that can be harvested (Bellasio and Lundgren, 2016). It was proposed that any shift in ATP and NADPH availability between M and BS can be to some extent countered by adjusting ATP and NADPH demand (Bellasio and Griffiths, 2014c). The extensive overlap between BS and M functions, for instance, the capacity to synthesize starch (Spilatro and Preiss, 1987, Kanai and Edwards, 1999), reduce phosphoglyceric acid, PGA (Majeran and van Wijk, 2009), regenerate PEP through PPDK (Aoyagi and Nakamoto, 1985), or PEPCK (Wingler *et al.*, 1999) may all concur to this rearrangement (Weber and von Caemmerer, 2010, Bellasio, 2017).

We have shown in the companion paper that the photosynthetic apparatus of *Setaria viridis* rearranges in response to low light in a cell-specific fashion, preferentially increasing electron transport capacity in BS cells (Ermakova *et al.*, 2021). Here we study how changes of electron transport contribute to light acclimation at leaf level. First, we measure anatomical properties of leaves grown under high light (HL) and low light (LL) and estimate how these would influence light harvesting of the M and the BS. Then, we conduct a comprehensive gas-exchange characterisation under ambient and low O_2, with concurrent determination of Photosystem II (PSII) and PSI effective quantum yields, to estimate biochemical parameters and conductance to CO_2 diffusion at the M/BS interface (g_{BS}). Finally, we develop a novel model integrating two electron transport chains with the light harvesting properties of M and BS to study how the apportioning of light and dark reaction shifts in LL plants, and how these changes affect biochemical efficiency.

Methods

Plants

Plants of *S. viridis* (A10 ecotype) were grown in 2 L pots in controlled chambers with 16 h illumination at the intensity of 1000 µmol m^{-2} s^{-1} or 300 µmol m^{-2} s^{-1}, chosen to avoid severe photosynthetic impairment which may arise under deep shade, and reached by covering part of the cabinet with shade cloth; 28°C day, 24°C night, and 60 % humidity. All measurements were performed on the youngest fully expanded leaves sampled before flowering between 15 and 25 days after germination. Analyses were conducted before flowering (15–25 days post germination) on young fully expanded leaves.

Leaf anatomy

Resin–embedded cross–sections were prepared and imaged according to Pengelly *et al.* (2010). Quantification of anatomical parameters was performed using Image J software (NIH, WI) on an equal number of secondary and tertiary veins as described in Bellasio and Lundgren (2016). Calculations of mesophyll surface area exposed to intercellular airspace (S_m) and bundle sheath cells surface area per unit of leaf area (S_b) were made as described in Pengelly *et al.* (2010) using the curvature correction factor of 1.43 from Evans *et al.* (1994).

Chlorophyll

Total chlorophyll was extracted from frozen leaf discs ground using TissueLyser II (Qiagen, Venlo, The Netherlands) or from protein samples in 80% acetone, buffered with 25 mM 4-(2-hydroxyethyl)-1-piperazineethanesulfonic acid (Hepes)-KOH (pH 7.8). Chlorophyll *a* and *b* content was measured at 750 nm, 663.3 nm and 646.6 nm, and calculated according to Porra *et al.* (1989). Chlorophyll *a*/*b* ratios were determined for BS cells directly from isolated BS strands, while M cell ratios were determined from the mesophyll sap released upon leaf rolling as described in Covshoff *et al.* (2012). The fraction of total leaf chlorophyll in BS cells was calculated as x from: $a\,x + b\,(1\text{-}x) = c$, where a is the chlorophyll *a*/*b* ratio of BS cells, b is the chlorophyll *a*/*b* ratio of M cells, and c is the chlorophyll *a*/*b* ratio of leaf.

Westerns blotting and immunolocalisation

Protein isolation from leaves, gel electrophoresis and western blotting were performed as described in Ermakova *et al.* (2019). PEPCK antibodies (Agrisera, Vännäs, Sweden) were used according to the manufacturer's protocol. Immunolocalisation of PPDK was performed after

(Ermakova *et al.*, 2020) on lightly fixed leaf cross-sections. Sections were treated with the PPDK primary antibody (1:100, Agrisera), Alexa Fluor 488–conjugated goat anti-rabbit secondary antibody (1:200, Life Technologies, Eugene, OR) and 0.05 % calcofluor white to stain cell walls. Fluorescence signal was captured with the Leica DM5500 microscope (Leica, Wetzlar, Germany) equipped with the Leica DFC7000T camera using the Leica Application Suite 4.12 software. Fluorescence was detected at 505–565 nm for PPDK (excitation 490–510 nm, YFP Filter Cube, Leica) and at 450–490 nm for cell walls (excitation 330–370 nm, A4 Filter Cube, Leica).

Simultaneous gas exchange, chlorophyll fluorescence and P700 measurements

Gas exchange, fluorescence and P700 were measured simultaneously on leaves aligned without overlapping their edges to fill the cuvette with the setup of Bellasio and Farquhar (2019). Briefly, a portable gas exchange system (LI6400XT, Li–Cor, Lincoln, NE) was modified to operate at low CO_2 concentrations (see licor.com) and fitted with a 6400–06 PAM2000 adapter (courtesy of Susanne von Caemmerer), holding a fibre probe in the upper leaf cuvette distant enough to minimise shading. Light was provided by a bespoke red–blue light source, positioned to illuminate uniformly the leaf. Light intensity was measured through an in–chamber Gallium arsenide photodiode, calibrated using a Li–250 light sensor (Li–Cor). Neoprene gaskets were used on both sides of the cuvette. A mixture of 2 % O_2 was prepared by mixing ambient air and N_2 with a bespoke gas mixing unit (kindly assembled by Suan Chin Wong). This mix or ambient air was CO_2–scrubbed with soda lime and humidified to a dew point of 15–17 °C upstream of the inlet to maintain water vapour pressure deficit around 1 kPa. CO_2 was added from a large cylinder (BOC, St Peters, Australia), using the CO_2 injection unit of the LI6400XT. Mass flow leaks (Boesgaard *et al.*, 2013) were monitored with a gas flow meter as detailed in Bellasio *et al.* (2016b).

PSII and P700 yields were measured with a Dual PAM–F (Heinz Walz GmbH, Effeltrich, Germany, courtesy of Dean Price). Saturating pulse intensity was set at 20,000 µmol m^{-2} s^{-1} to saturate the fluorescence signal. P_M, the maximal level of P700 oxidation, and P_0, the minimal P700 signal were recorded when saturating pulse was given after pre-illumination with far-red light. Photosynthetic parameters (P, steady-state P700 signal; P_M', maximal P700 signal; F, steady-state fluorescence signal, F_M', maximal fluorescence signal) were monitored by the saturating pulse application at different irradiances, CO_2 and O_2 concentrations. The effective quantum yield of PSII [*Y(II)*] was calculated according to Genty *et al.* (1989). The effective quantum yield of PSI [*Y(I)*], the non-photochemical yield of PSI caused by donor side

limitation [*Y(ND)*] and the non-photochemical yield of PSI caused by acceptor side limitation [*Y(NA)*] were calculated as described in Klughammer and Schreiber (2008).

Four photosynthetic response curves (*A*/*PPFD* and *A*/C_i curves, under ambient and low [O_2]) were measured at 25 °C in daylong experiments. *A*/C_i curves were measured first, under a *PPFD* of 1000 µmol m^{-2} s^{-1}, *A*/*PPFD* curves were measured under reference [CO_2] of 420 µmol mol^{-1}. The order between ambient and low O_2 was inverted each day. Flow rate was 400 µmol s^{-1}; CO_2 diffusion through the gaskets was compensated by lengthening the tubing of the LI6400XT reference gas (Bellasio and Farquhar, 2019). Gas response curves were analysed using the protocol of Bellasio *et al.* (2016a), assumptions are detailed in Note S6. CO_2 concentration at the M carboxylation sites was calculated as $C_M = C_i - A/g_M$, where mesophyll conductance (g_M) was 1.5 for HL and 1.2 mol m^{-2} s^{-1} for LL derived by adjusting for S_m (Table 1) the data of Ubierna *et al.* (2017).

C_4 photosynthesis model

A novel steady-state model of C_4 photosynthetic carbon metabolism, including key reactions involved in the reductive pentose phosphate (RPP) cycle, photorespiration pathway and carbohydrate synthesis, was originally developed to simulate assimilatory responses of HL and LL plants. The initial assumptions are described in Note S1, the overall schematics are shown in Figure 2 and Figure S1. Briefly, the biochemical space forms a continuum that can be explored by varying two parameters: f_{MDH}, representing the engagement of MDH in M cells (in this study we used the discrete value of one), and f_{PEPCK}, the capacity of PEPCK to consume ATP available in BS cells. Light reactions are described separately for M and BS compartments, accounting for the light absorption partitioning ($AB\ \frac{BS}{M}$) that was derived from the light absorption in the leaf profile following Bellasio and Lundgren (2016), and parameterised with measured chlorophyll concentration in the M and the BS, and anatomical characteristics (Table 1). Light reactions incorporate the pathway through the chloroplastic NAD(P) dehydrogenase complex (NDH) and the model allows for variation in the ratio of ATP/NADPH production rates via adjustment of CEF, while keeping total light absorption constant (Bellasio, 2019). The reducing power requirements for nitrogen reduction and for the water-water cycle are explicitly accounted for as a fraction of pseudo-cyclic electron flow, after Yin and Struik (2012) as modified by Bellasio (2019). The model uses mesophyll [CO_2] (C_M) as an input. Supply of ATP from light reactions and demand from dark reactions are linked through stoichiometric functions solved explicitly for the reaction rates, and CO_2 and O_2

concentrations in M and BS compartments, separately (Note S3). Reducing power poise (Note S4) and metabolite flows (Note S5) are calculated through a set of stoichiometric constraints based on Bellasio (2017). Details of parameterisation are in Note S6 and Table S1; model sensitivity is shown in Table S2; comparison with other models is made in note S7.

Statistical analysis

The relationship between mean values for HL and LL plants was tested using a two-tailed, heteroscedastic Student's *t*-test (Microsoft Excel® 2016).

Results

Leaf anatomy and chlorophyll

In HL plants BS cells chloroplasts were uniformly distributed inside the cells (Figure 1). In LL plants M cells had chloroplasts specifically arranged along the cell walls particularly in adaxial M cells. In LL plants BS chloroplasts had clear centrifugal position and adaxial BS cells had more chloroplasts compared to abaxial BS cells than in HL plants, resulting in higher chlorophyll content in the BS of LL plants relative to the M (Table 1). LL leaves had 15 % lower M thickness as well as 10 % lower interveinal distance compared to HL. BS surface area per leaf area (S_b) was 13 % lower in LL plants, and M surface area exposed to the intercellular airspace (S_m) was 35 % lower than in HL plants.

Gas-exchange and yield of photosystems

When the light–response was measured at 420 µmol mol^{-1} CO_2 and 21 % O_2, no difference was significant between HL and LL plants in CO_2 assimilation rate (*A*) or effective quantum yields of PSII [*Y(II)*] and PSI [*Y(I)*] (Figure 3). Yields of non-photochemical losses in PSI due to the donor [*Y(ND)*] and acceptor [*Y(NA)*] side limitations did not differ between the two growth regimes (Figure 3g). At 2 % O_2, no differences in light responses between HL and LL plants were detected (Figure 4). Interestingly, a decrease of *Y(I)* at low irradiance underpinned by an increase of *Y(NA)* (unavailability of PSI acceptors) was greater under 21 % O_2 (Figure 3e, Figure 4e).

CO_2 response curves were measured at a *PPFD* of 1000 µmol m^{-2} s^{-1} either at 21 % or 2 % O_2. No differences in CO_2 assimilation, *Y(II)*, *Y(I)*, *Y(ND)* or *Y(NA)* were significant between HL and LL plants independently of O_2 level (Figure 3, Figure 4). Both HL and LL plants showed an increasing trend of *Y(ND)* for decreasing C_M. This mechanism of PSI

photoprotection, known as the photosynthetic control, has been extensively studied in C_3 plants. The acidification of the thylakoid lumen – due to the reduction in the turnover of ATP synthase limited by ADP and phosphate availability – slows down the plastoquinol oxidation by Cytochrome b_6f (Tikhonov, 2014). In addition, the acidification of the lumen induces the non–photochemical energy dissipation in the PSII antennae (Li *et al.*, 2004); these processes downregulate PSI by keeping the donor side of P700 reaction centres more oxidised, seen as increase of *Y(ND)*. Interestingly, *Y(NA)* at low C_M was higher when measured at 2 % O_2 (Figure 3h, Figure 4h), pointing to a contribution of O_2 to oxidation of PSI at limiting CO_2 via photorespiration and/or O_2 photoreduction also shown previously in C_3 plants (Takagi *et al.*, 2016).

For detailed analysis of the measured light and CO_2 response curves we fitted empirical and mechanistic models after Bellasio *et al.* (2016a). Outputs in Table 2 show that under ambient O_2 the main differences were dependent on a decrease of respiration in the light (R_{LIGHT}), light compensation point (*LCP*), CO_2 compensation point (Γ) and BS conductance to CO_2 diffusion (g_{BS}) in LL plants. Curiously, O_2 sensitivity of R_{LIGHT}, quantum yield [$Y(CO_2)_{LL}$] and carboxylation efficiency was opposite between HL and LL plants. The decrease in photosynthetic efficiency in LL plants under low [O_2] may be due to a downregulation of PSII activity in the M as a response to the increased redox state of the plastoquinone pool caused by the reduced availability of O_2 as an electron sink; feedbacks of the thylakoid redox state on R_{LIGHT} are known to exist (Buckley and Adams, 2011), but not well characterised in C_4 plants.

Modelling of light distribution, light reactions and dark metabolism

Using measured anatomical characteristics and chlorophyll concentration (Table 1), we modelled light penetration through the leaf profile according to Bellasio and Lundgren (2016). Absorbed light in the BS relative to M was higher in HL plants ($AB\ \frac{BS}{M}$ was 0.414 for HL and 0.343 for LL, Table 1). Next, to gain comprehensive understanding of the photosynthetic metabolism, we used these values and the quantities derived from the concurrent gas–exchange and chlorophyll fluorescence measurements (See Note S6 and Table S1) to parameterise a model of light reactions and dark metabolism (Notes S1–S5), while the fraction of electron flow through PSI following CEF in M and BS ($f_{Cyc\ M}$ and $f_{Cyc\ BS}$, respectively) were fitted to maximise assimilation, constrained to maintain PPDK and PEPCK activity in BS cells at zero (Figure 5 and 6).

Initially, we replicated *in silico* the leaf gas–exchange measurements under ambient O_2 level (Figure 3). Both for light and CO_2 response curves, the trends of CO_2 assimilation and *Y(II)* were well captured by the model. In the light response curves the model captured a hyperbolic decrease of the measured *Y(I)* at high irradiance (Figure 3e) but not an initial trough at low irradiance. However, the modelled *Y(I)* was similar to the trend of 1 - *Y(ND)*, perhaps only capturing the rate of *Y(I)* potentially available due to the electron input from PSII but not accounting for the loss of *Y(I)* due to the unavailability of acceptors [*Y(A)*]. In CO_2 response curves the hyperbolic increase of *Y(I)* was captured, but *Y(I)* was slightly underestimated for C_M greater than 20 µmol mol^{-1}. Predicted *Y(I)* did not differ between HL and LL plants.

Then, we carried out a complete characterisation of photosynthetic biochemistry using the specific parameterisation of growth light regimes (Table 3). In LL plants, there was a 60 % downregulation of assimilatory metabolism due to the lower energy available. Rubisco carboxylation (V_C), PEP carboxylation rate (V_P, which corresponds to the rate of malate export to BS cells and the backflux of pyruvate), all followed the same trend. The decrease in V_P caused a 25 % decrease in CO_2 concentration in the BS that was reflected by a higher ratio of Rubisco oxygenation relative to carboxylation (V_O/V_C, 4.9 % in HL plants and 5.4 % in LL plants). However, there was a general increase in PSII efficiency in LL plants which overweighed the effect on V_O/V_C: the average quantum yield increased 38 % on absorbed light basis (from 0.04 to 0.055 CO_2/quanta), and as much as 43 % on incident light basis (from 0.031 to 0.044 CO_2/quanta). This difference was due to the higher leaf absorbance of LL plants (captured in the measurements by *s'*, Table 2, and in the model inputs by *s*, Table S1).

Discussion

Setaria viridis is a wild ancestor of *S. italica* (foxtail millet), a grain crop widely grown in China and India (Li and Brutnell, 2011), and has gained favour for studying C_4 photosynthesis because it has a rapid life cycle, small stature, sequenced genome and available genetic transformation method (Brutnell *et al.*, 2010). Since C_4 photosynthesis has evolved independently around 70 times (Sage *et al.*, 2011, Sage, 2017), diverse arrangements can be expected between C_4 plants, and characterising variability of acclimation to shade is prerequisite for identifying best targets for improving crop performance. While anatomical responses of C_4 plants to shading are relatively conserved [Table 1, *e.g.* (Ward and Woolhouse, 1986, Pengelly *et al.*, 2010)], biochemical strategies appear to be diverse.

We showed that *S. viridis* grown at limiting irradiance deployed a suite of protein level adjustments providing BS thylakoids with increased capacity for light harvesting and electron

transport pointing to an increased ATP demand in the BS (Ermakova *et al.*, 2021). Here, we were interested in how those modifications would upscale to the leaf level and rearrange the partitioning of biochemical work between M and BS. Whilst acclimation to LL generally entails a downregulation of photosynthetic potential, here gas exchange measurements showed that HL and LL plants reached strikingly similar rates of assimilation regardless of light or CO_2 levels. This intriguing invariance, which we repeatedly measured in plants from different growth batches, and was previously independently observed in the same ecotype (Henry *et al.*, 2019), may be a particular feature of *S. viridis*. Detailed analysis of the response curves through model fitting (Table 2) revealed contrasting strategies of acclimation. LL plants had lower carboxylation efficiency and lower $Y(II)_{LL}$, but also lower respiration than HL plants. We then characterised the leaf anatomy and found a reduction in BS size in LL plants, and a reduction in BS surface area per leaf area (S_b), which presumably concurred to the reduction of g_{BS} (von Caemmerer *et al.*, 2008), here estimated by fitting of gas exchange and fluorescence data obtained under ambient and low [O_2]. The reduction of g_{BS} at low light is consistent with previous results obtained through different proxies including anatomy, isotopic discrimination, combined gas exchange and chlorophyll fluorescence (Pengelly *et al.*, 2010, Ubierna *et al.*, 2013). Interestingly, g_{BS} had been estimated to decrease both in plants grown under low light (Bellasio and Griffiths, 2014b) and in plants grown under high light subsequently transferred to low light as it occurs in crop canopies where older leaves are shaded by new growth (Bellasio and Griffiths, 2014a).

The decrease in g_{BS} ameliorates the efficiency of C_4 assimilation. By hindering CO_2 leakage it counters the decrease in CO_2 concentration in the BS and the increase of photorespiration occurring under low light (Kromdijk *et al.*, 2014). However, the associated reduction in BS size (Table 1) has the undesirable consequence of decreasing the light harvesting in BS cells, limiting ATP generation and decreasing the operational plasticity under changing light conditions (Bellasio and Lundgren, 2016). LL plants deployed a concerted suite of responses to counter potential ATP starvation in the BS. Firstly, the arrangement of M chloroplasts appressed to the cell walls (Figure 1), similar to that observed in *Saccharum officinarum* grown under low light (Sales *et al.*, 2018), created optical gaps, increasing the amount of light filtering through to BS cells, a phenomenon known as the 'sieve effect' (Terashima *et al.*, 2009), while in HL plants M chloroplasts were dispersed. Rapid movement of M chloroplasts in response to HL is mediated by a blue light receptor and influenced by the presence of abscisic acid but not by the circadian clock (Maai *et al.*, 2020a). Chloroplasts arrangements are diverse depending on species, light quality and intensity. For instance, under midday illumination *Eleusine*

coracana was shown to aggregate M chloroplasts around the BS; *Zea mays* showed a dispersed arrangement, similar to what we observed in *S. viridis*; *Sorghum bicolor* created characteristic optical corridors spanning the whole leaf thickness, presumably aiding photoprotection, observed also in *Z. mays* but only under non–physiological irradiance (3,000–4,000 µmol m^{-2} s^{-1}) (Yamada *et al.*, 2009, Maai *et al.*, 2020a, Maai *et al.*, 2020b). Secondly, the BS had higher chlorophyll content (Table 1), lower chlorophyll *a*/*b* ratio and higher abundance of light-harvesting complexes (LHC) I and II than HL plants (Ermakova *et al.*, 2021). Consistently, curve fitting of combined gas exchange and fluorescence data captured a higher s′, the parameter representing effective leaf level light interception lumped to the yield of ATP generation (Table 2). Thirdly, the potential of BS thylakoid membranes for ATP production increased due to the upregulation of PSI, ATP synthase and NDH (Ermakova *et al.*, 2021). The latter has been shown to be beneficial for C_4 photosynthesis in reverse genetics studies (Ishikawa *et al.*, 2016, Peterson *et al.*, 2016) and found to correlate with the ATP requirements of the cell types in C_4 plants (Takabayashi *et al.*, 2005).

Next, we were interested in resolving to what extent the observed reorganisations of light harvesting and electron transport processes in LL plants was effective in countering the limitations to ATP generation caused by a smaller BS, and what modifications to the metabolism of BS and M were required to maintain invariant levels of assimilation (Figure 3). We developed a novel model encompassing explicit anatomy and separate electron transport chains in the BS and in the M, parameterised specifically for HL and LL plants. We found that the increased chlorophyll concentration was not sufficient to counter the effect of smaller BS cells size, and, overall, LL plants absorbed 40 % less light in BS cells relative to total (from 23 % under HL to 14 % under LL, Table 3). However, the higher proportion of CEF (f_{Cyc}) in BS of LL plants (Figure 6) could partially compensate for the decrease in light absorption so that the predicted ATP production rate, relative to total, only decreased 5 % (from 45 % in the BS of HL plants to 42 % in the BS of LL plants, Table 3). The predicted changes in f_{Cyc} were supported by the detected BS/M redistribution of NDH (Ermakova *et al.*, 2021), but, importantly, the simulations were independent of protein data. Hence, we demonstrated that first, the upregulation of CEF (f_{Cyc}) is effective in mitigating decreased light interception in BS cells; and, second, that decreasing light interception in BS cells is a sufficient condition to justify upregulation of f_{Cyc}. To our knowledge this functional dependence is demonstrated here for the first time, uncovering another important link between biochemical properties and structural characteristics of C_4 leaves.

The NADPH production rate in BS cells relative to total was predicted to decrease 97 % in LL plants (from 11 % under HL to 0.3 % under LL), driven both by the decrease in BS size and increase in f_{Cyc}. This led to a 13 % decrease in the rate of PGA reduction in BS cells relative to total (from 66 % under HL to 59 % under LL), and a consequent relative increase of triose fluxes between M and BS cells in LL plants (Table 3). By means of LEF, PSII activity in BS cells not only supplies NADPH production, but also replenishes CEF electrons leaking to various electron sinks downstream of PSI (explicitly accounted for in the model as pseudocyclic electron flow). In this model LEF (J_2) in the BS was predicted to be 21 µmol m^{-2} s^{-1} (14 % of the total leaf rate for HL plants), and 5.59 µmol m^{-2} s^{-1} (9 % of the total leaf rate for LL plants, Table 2). Whilst the actual PSII activity measured from the BS thylakoid membranes of LL plants was circa 7 % of the leaf rate, therefore matching the predicted value, the actual PSII activity in BS cells of HL plants was much lower (Ermakova *et al.*, 2021), meaning that the predicted value of J_2 cannot be supplied *in vivo* by electrons coming from the water oxidation. Therefore, the predicted rate of J_2 in BS cells of HL plants must be obtained via oxidation of NADPH derived from malate imported from the M, and supplying electrons to plastoquinone through the NDH. Indeed, when supplied with malate, isolated BS strands of *Z. mays* retained PSI activity even in the presence of PSII inhibitor and the BS of *S. bicolor* maintained CO_2 fixation under far–red illumination, unable to excite PSII (Osmond, 1974, Ivanov *et al.*, 2005).

Theory had shown that, under changing irradiance, flexibility in the apportioning of PGA reduction between BS and M cells can regulate the BS demand of NADPH, and the engagement of PEPCK and PPDK can attune the BS demand of ATP (Furbank, 2011, Bellasio and Griffiths, 2014c). Indeed, NADP–ME plants like *Z. mays* and *S. officinarum* acclimated to low light, increased the total rate of PEPCK activity (Sales *et al.*, 2018), or the activity of PEPCK relative to PEPC (Sharwood *et al.*, 2014, Sonawane *et al.*, 2018), and increased the pool of inactive PEPCK (B.V. Sonawane, personal communication), presumably available to be activated by changing light conditions (Bailey *et al.*, 2007). Because PEPCK consumes ATP generated in the M and is tightly regulated by ATP concentration, the expression of PEPCK in NADP–ME plants was predicted to increase light harvesting plasticity, *i.e.* the capacity to efficiently harvest light in a broad range of intensity and spectral quality (Bellasio and Griffiths, 2014c). Further, the activity of PPDK in the BS could compensate for a lack of PEPCK, making PEPCK engagement necessary when the activity of PPDK in the BS was reduced, and *vice versa* (Bellasio, 2017).

Uniquely, *S. viridis* did not express PEPCK neither under HL nor under LL (Figure 5). Nor we found detectable levels of PPDK in the BS (Figure 5), in line with previous reports (John *et al.*, 2014, Schlüter and Weber, 2020). *Z. mays* grown under low light although overexpressed LHCII subunits and PsbD in BS cells (Drozak and Romanowska, 2006), did not show oxygen activity or changes in supramolecular organisation of PSII (Romanowska *et al.*, 2006, Rogowski *et al.*, 2019). In contrast, *S. viridis* had a striking plasticity in acclimating light reactions, probably sufficient to avoid the necessity to regulate PEPCK and PPDK expression (Figure 5). Importantly, and differently from the nine species (four NADP–ME including *Z. mays* and *S. bicolor*, two NAD–ME, two PEPCK) studied by Sonawane *et al.* (2018), acclimation of light reactions in *S. viridis* did not compromise quantum yield (Table 2). Therefore, the outstanding capacity of *S. viridis* to rearrange light reactions under low light is a highly efficient acclimation strategy setting *S. viridis* aside from other NADP–ME plants, and representing a novel – so far overlooked – innovation in C_4 evolutionary history.

Conclusion

Previous reports have proposed that dark reactions of C_4 photosynthesis could be adjusted to cope with low irradiance, by regulating the rate of PGA reduction and PEPCK or PPDK activity in the BS. *S. viridis* did not regulate PEPCK and PPDK but, instead, adjusted electron transport processes. Using a new model, we analytically and mechanistically solved the causality link between anatomy and biochemistry: a given optical cross section determined the absorption of light in the BS and the M, the rate of electron transport, the engagement of CEF and LEF, the rate of ATP and NADPH generation, and ultimately the apportioning of dark reactions between M and BS cells. Although quantifying the impact to field conditions will require additional experiments, the striking capacity of *S. viridis* to acclimate light reactions presents a novel and perhaps the most efficient shade tolerance strategy, potentially leading to novel possibilities for crop improvement.

Availability

Data and the model, coded in Microsoft® Excel®, are made freely available in the Supporting Information.

Author contributions

412 ME and CB conceived the project. CB developed the model and ran simulation. CB and
413 ME performed experiments, analysed the data and wrote the article. Authors have no conflict
414 of interest.

415 **Acknowledgements**

416 We are deeply grateful to Graham Douglas Farquhar for hospitality, to Suan Chin Wong
417 and Dean Price for equipment, to Susanne von Caemmerer for critical review and equipment.
418 We thank Florence Danila, Joanne Lee and Centre for Advanced Microscopy at the Australian
419 National University for preparing and imaging leaf cross-sections. We thank Balasaheb Vitthal
420 Sonawane for data and discussion, Riya Kuruvilla for immunolocalisation assay and Tegan
421 Norley for anatomical measurements. We thank the Australian Plant Phenomics Facility
422 supported under the National Collaborative Research Infrastructure Strategy of the Australian
423 Government. CB is funded by H2020 Marie Skłodowska-Curie individual fellowship
424 (DILIPHO, ID: 702755). ME is supported by the Australian Research Council Centre of
425 Excellence for Translational Photosynthesis (CE140100015).

426

Table 1. Anatomical and biochemical characteristics of leaves, mesophyll (M) and bundle sheath (BS) cells of *S. viridis* grown at high light (1000 µmol m^{-2} s^{-1}, HL) or low light (300 µmol m^{-2} s^{-1}, LL). Mean values are shown ± SE, $n = 20$. Asterisks indicate statistically significant difference between two light regimes ($P < 0.05$).

Characteristic	HL	LL
Height at vein (µm)	238 ±12.2	205 ±8.5*
Interveinal distance (µm)	181.5 ±4.8	165 ±4.8*
Abaxial Mesophyll Height (µm)	60.2 ±3.3	46.0 ±2.5*
Adaxial Mesophyll Height (µm)	68.8 ±3.2	69.7 ±3.7
Bundle sheath area (µm²)	9604 ±1101	6719 ±763*
Vein width (µm)	98.1 ±6.5	89.1 ±5.11
Chlorophyll (*a*+*b*) in the BS relative to M $\left(\frac{\text{mmol m}^{-2}\ \text{Leaf}}{\text{mmol m}^{-2}\ \text{Leaf}}\right)$	0.48	0.66
Absorbed light in the BS relative to M, $AB\ \frac{\text{BS}}{\text{M}}$,	0.414	0.343
Mesophyll surface area exposed to intercellular airspace, S_m (m^2 m^{-2})	14.13 ±0.4	9.12 ±0.5*
Bundle sheath cells surface area per unit of leaf area, S_b (m^2 m^{-2})	2.21 ±0.06	1.92 ±0.04*

Table 2. C_4 photosynthesis parameters obtained from curve fitting of gas-exchange responses of *S. viridis* grown at high light (HL) or low light (LL). $N = 3$ biological replicates, *p*–values in bold indicate statistically significant difference between two light regimes ($P < 0.05$).

			HL		LL		*p*–value
O_2	**Output**	**Description**	**Mean**	**SE**	**Mean**	**SE**	
21 %	R_{LIGHT} [1, a]	Respiration in the light	1.93	0.23	1.18	0.03	**0.03**
2 %	R_{LIGHT} [1, a]	Respiration in the light	1.70	0.29	1.43	0.02	0.25
21 %	$Y(II)_{LL}$ [2, a]	Initial yield of PSII extrapolated to *PPFD*=0	0.73	0.003	0.70	0.01	**0.04**
2 %	$Y(II)_{LL}$ [2, a]	Initial yield of PSII extrapolated to *PPFD*=0	0.64	0.04	0.69	0.001	0.18
21 %	*LCP* [1, b]	Light compensation point, i.e. *PPFD* when *A*=0	37.1	4.15	22.32	0.67	**0.02**
21 %	GA_{SAT} [1, b]	Light–saturated *GA*, under the CO_2 concentration of light–curves	459	8.5	421	29	0.18
21 %	$Y(CO_2)_{LL}$ [3, b]	Quantum yield for CO_2 fixation, i.e. quanta required for each CO_2 assimilated, extrapolated to *PPFD*=0; also known as Φ_{CO2LL}.	0.053	0.001	0.053	0.002	0.41
21 %	$PPFD_{50}$ [1, b]	*PPFD* that half saturates *GA*	37.3	0.50	35.8	1.4	0.24
21 %	*m* [2, b]	Curvature of the non–rectangular hyperbola describing the *PPFD* dependence of *GA*	0.70	0.04	0.75	0.02	0.19
2 %	*LCP* [1, b]	Light compensation point	34.2	4.7	25.8	0.37	0.11
2 %	GA_{SAT} [1, b]	Light–saturated *GA*	32.1	2.1	36.4	1.0	0.10
2 %	$Y(CO_2)_{LL}$ [3, b]	Quantum yield for CO_2 fixation	0.049	0.003	0.056	0.000	0.06
2 %	$PPFD_{50}$ [1, b]	*PPFD* that half saturates *GA*	370	32	407	20	0.24
2 %	*m* [2, b]	Curvature of the hyperbola	0.87	0.04	0.75	0.02	**0.04**
21 %	*CE* [4, b]	Carboxylation efficiency, i.e. initial slope of the A/C_i curve	0.68	0.03	0.70	0.02	0.36
21 %	A_{SAT} [1, b]	CO_2–saturated *A*, under the PPFD of *A*/*Ci* curves	28.0	0.32	28.1	0.27	0.44
21 %	ω [2, b]	Curvature of the non–rectangular hyperbola describing the C_i dependence of *A*	0.84	0.01	0.91	0.01	**0.01**
21 %	Γ [1, b]	C_i–A compensation point, i.e. C_i at which *A*=0	2.3	0.2	3.4	0.2	**0.01**
2 %	*CE* [4, b]	Carboxylation efficiency	0.75	0.01	0.62	0.01	**0.00**
2 %	A_{SAT} [1, b]	CO_2–saturated *A*	29.9	0.56	28.5	0.40	0.09
2 %	ω [2, b]	Curvature of the hyperbola	0.72	0.09	0.92	0.01	0.07
2 %	Γ [4, b]	C_i–A compensation point	2.6	0.2	3.1	0.3	0.18
2 %	*s'* [5, a]	ATP / Quanta (Yin *et al.*, 2011)	0.222	0.01	0.243	0.002	0.11
21 %	J_{ATPSAT} [1, c]	Light–saturated ATP production rate	219	26	194	11	0.25
21 %	θ [2, c]	Curvature of the non–rectangular hyperbola describing the *PPFD* dependence of J_{ATP}	0.67	0.1	0.71	0.05	0.38
21 %	$PPFD_{50}$ [1, c]	*PPFD* which half saturates J_{ATP}	553	95	441	42	0.21
21%	g_{BS} [4, d]	BS conductance to CO_2 diffusion	0.0018	0.0002	0.0012	0.0001	**0.02**
21 % and 2 %	V_{PMAX} [1, e]	Maximum PEPC carboxylation rate	163	12	164	7.4	0.48

Method: [a] linear fitting of gas exchange and fluorescence (Yin *et al.*, 2011) following Bellasio *et al.* (2016a); [b] Fitted non–rectangular hyperbola (Bellasio *et al.*, 2016b); [c] non–linear calibration of Bellasio and Griffiths (2014b); [d] concurrent fitting of A/C_i and light curves under light limited conditions using non-linear estimates of J_{ATP} using the model of von Caemmerer (2000), following Bellasio and Griffiths (2014b) and Bellasio *et al.* (2016a); [e] concurrent fitting of 2 % and 21 % O_2 using the model of von Caemmerer and Furbank (1999), following Bellasio *et al.* (2016a). Units: [1] µmol m^{-2} s^{-1}; [2] Dimensionless; [3] CO_2/quanta; [4] mol m^{-2} s^{-1}

Table 3. Output of the combined light reaction and biochemical model of C_4 photosynthesis. The output shown is calculated at the growth *PPFD* (1000 for HL or 300 µmol m^{-2} s^{-1} for LL), and expressed, except for f_{Cyc} (dimensionless) and *C* (µmol mol^{-1}), in µmol m^{-2} s^{-1} and in brackets as a fraction of gross assimilation at the growth light (30.97 for HL and 13.24 µmol m^{-2} s^{-1} for LL plants).

		HL		LL	
Symbol	**Description**	**M**	**BS**	**M**	**BS**
f_{Cyc}	Fraction of electron flow through PSI (J_1) following CEF	0.01	0.783	0.08	0.866
C	CO_2 concentration	400	4100	400	3100
I_{Inc}	Incident light (*PPFD*)	707 (23.5)	293 (9.71)	223 (17.7)	77 (6.08)
I_2	Light absorbed by PSII	310 (10.0)	50 (1.63)	100 (7.54)	9.5 (0.718)
I_1	Light absorbed by PSI	238 (7.68)	176 (5.69)	79.1 (5.97)	51.9 (3.92)
J_2	Electron flow through PSII	151 (4.88)	25 (0.794)	63.8 (4.82)	6.07 (0.458)
J_1	Electron flow through PSI	153(4.92)	113 (3.65)	69.2 (5.22)	45.4 (3.43)
J_{NADPH}	NADPH production rate (half the electron flow to NADPH)	58.8 (1.90)	7.09 (0.229)	27.4 (2.07)	0.948 (0.07)
J_{ATP}	ATP production rate	97.9 (3.16)	80.2 (2.59)	44.2 (3.34)	32.5 (2.46)
V_P	PEP carboxylation rate. Because in this study f_{MDHM}=1, V_P corresponds to the rate of malate flux to the BS, the rate of pyruvate flux to the M, the PPDK reaction rate in the M (PPDK reaction rate in the BS is fitted to be zero in this study) and the malic enzyme reaction rate	36.7 (1.18)	0	15.9 (1.20)	0
L	Leakage rate of CO_2 out of the BS	6.64 (0.214)		3.21 (0.242)	
Φ	Leakiness: CO_2 leakage rate out of the BS relative to V_P	0.18		0.20	
V_C	Rubisco rate of carboxylation	0	31.7 (1.02)	0	13.6 (1.03)
V_O	Rubisco rate of oxygenation	0	1.54 (0.0496)	0	0.735 (0.0555)
PR	Rate of PGA reduction	22.2 (0.716)	43.0 (1.39)	11.5 (0.868)	16.4 (1.24)
$DHAP_{RPP}$	Rate of DHAP entering the conversion phase of the RPP cycle	0	55.5 (1.79)	0	23.9 (1.81)
RuP_{Phosph}	Rate of RuP phosphorylation	0	33.3 (1.07)	0	14.3 (1.08)
CS	Rate of carbohydrate synthesis	4.85 (0.156)	4.85 (0.156)	2.01 (0.152)	2.01 (0.152)
R_{Light}	Rate of respiration in the light	0.95 (0.031)	0.95 (0.031)	0.590 (0.047)	0.590 (0.046)
PGA flux	Flux of PGA	22.5 (0.726)	-22.5 (-0.726)	11.7 (0.882)	-11.7 (-0.882)
DHAP flux	Flux of DHAP	-17.3 (-0.559)	17.3 (0.559)	-9.48 (-0.716)	9.48 (0.716)

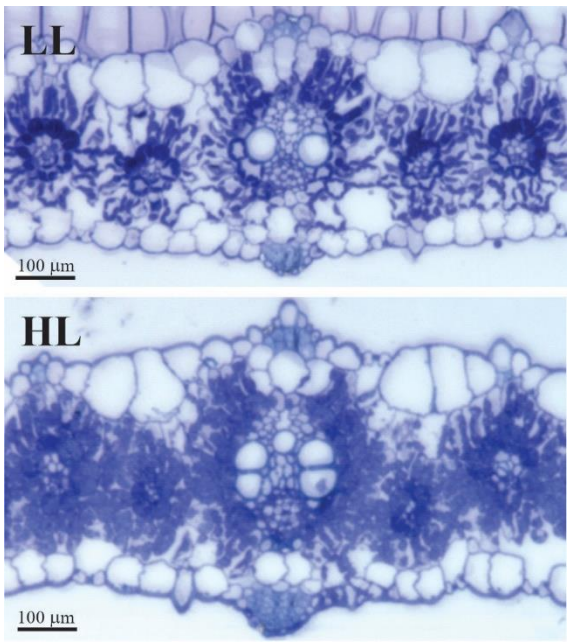

Figure 1. Light microscopy images of the leaf cross-sections used for anatomical measurements from *S. viridis* grown under high light (1000 µmol m^{-2} s^{-1}, HL) or low light (300 µmol m^{-2} s^{-1}, LL).

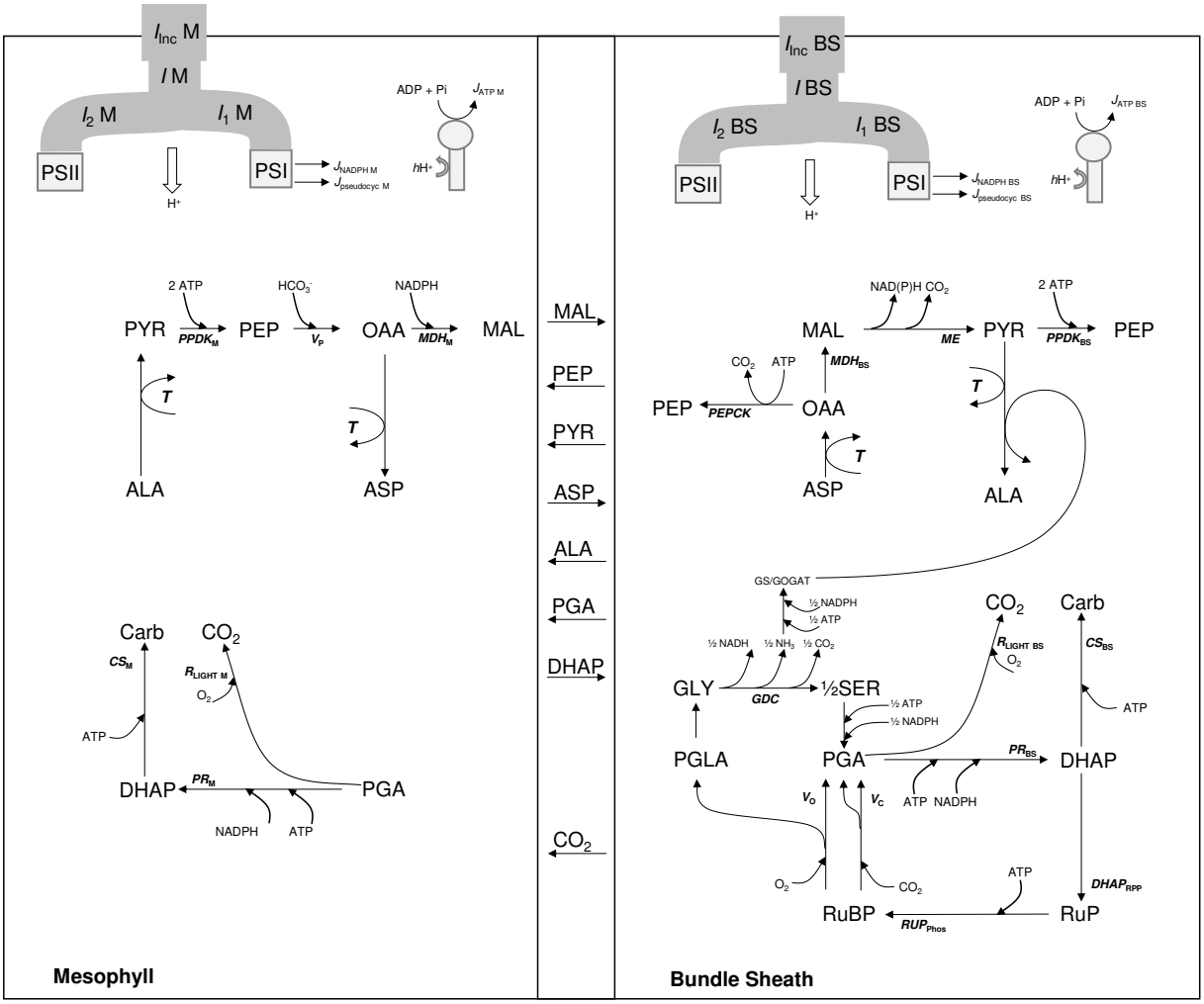

Figure 2. C_4 photosynthesis model schematic. The leaf is divided into M and BS compartments. Incident light (*PPFD* or I_{inc}) may reach M ($I_{Inc\ M}$) or BS cells ($I_{Inc\ BS}$) depending on anatomical characteristics and size of the light harvesting machinery. A fraction I is absorbed by PSI or PSII (I_1 or I_2, respectively). Light reactions (Fig. S1) result in the production of NADPH and ATP, which are consumed by dark reactions encompassing C_4 and C_3 activity. C_4 reactions are schematised in the middle. CO_2 is initially fixed by PEP carboxylase (PEPC) at the rate V_P to form oxaloacetate (OAA). This may be reduced to malate (MAL) or to aspartate (ASP) which both diffuse to BS cells. ASP is transaminated and may be decarboxylated by PEP carboxykinase (PEPCK) or by malic enzyme (ME). The regeneration of PEP used by PEPC is shared between M and BS cells depending on energy availability. The C_3 metabolism appears at the bottom, partitioned between M and BS compartments. Rubisco carboxylation and oxygenation reactions (V_C and V_O) consume RuBP and produce PGA and PGLA and are fully compartmentalised in BS cells. PGLA is recycled through the photorespiration cycle eventually regenerating PGA. This is a substrate of respiration (R_{LIGHT}) and is reduced (*PR*) to triose phosphate (DHAP), which is a substrate of carbohydrate synthesis (CS), the final product of photosynthesis, a generic triose that vanishes once synthesised. The majority of DHAP enters the sugar conversion phase of the reductive pentose phosphate (RPP) cycle. Metabolites for which fluxes are calculated are listed in the middle. The Excel workbook provided renders outputs according to this scheme.

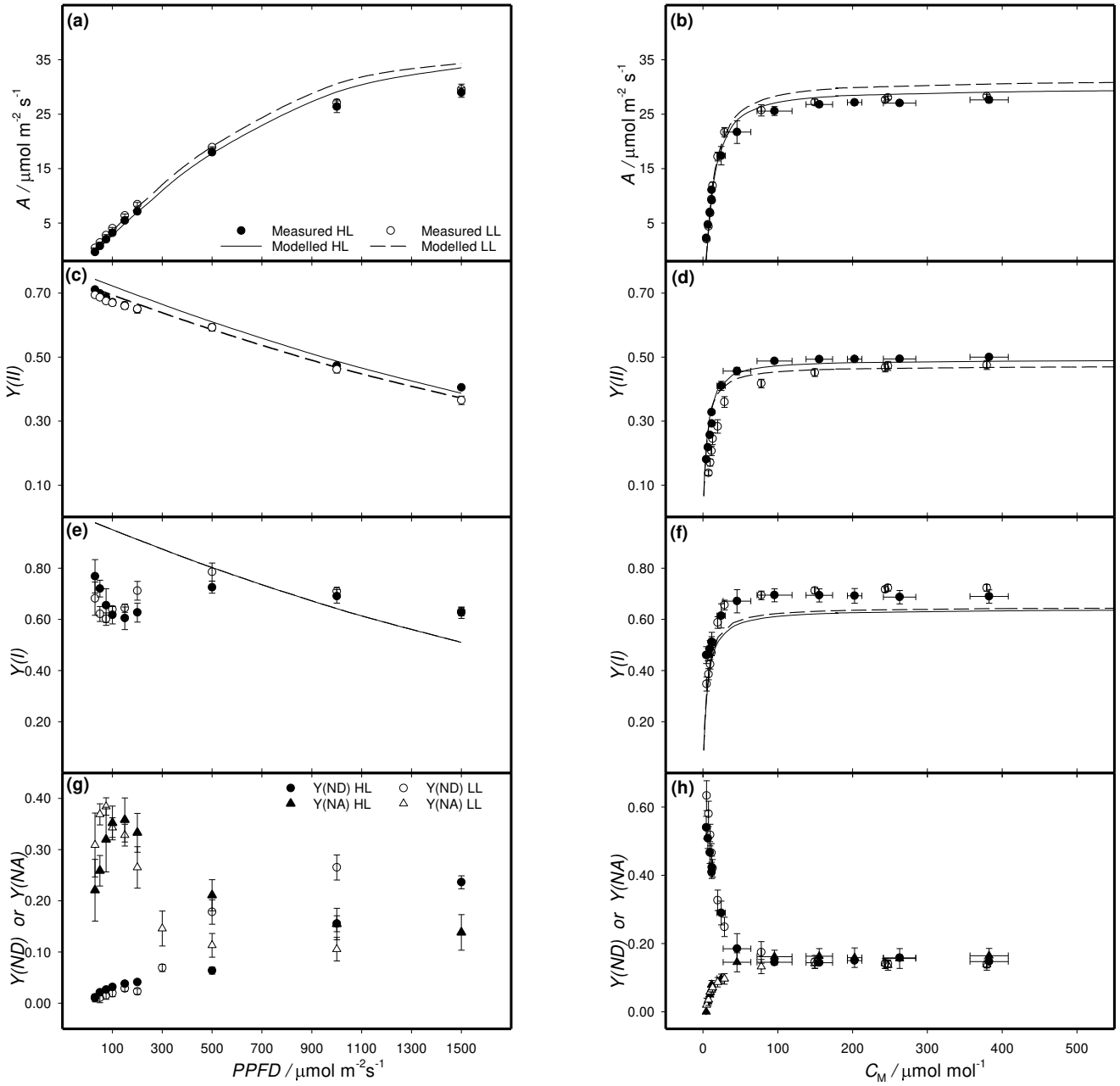

Figure 3. Measured and modelled gas-exchange and photosystems yield under ambient O_2 level. Symbols show response curves of CO_2 assimilation (**a**, **b**), quantum yield of Photosystem II (**c**, **d**), quantum yield of Photosystem I (**e**, **f**), Photosystem I donor [*Y(ND)*] and acceptor side [*Y(NA)*] limitations (**g**, **h**) obtained for *S. viridis* grown at high light (HL, solid circles) and low light (LL, empty circles). Light curves measured under a reference [CO_2] of 420 µmol mol^{-1} are shown in left panels, and CO_2 response curves obtained under constant irradiance of 1000 µmol m^{-2} s^{-1} are shown in right panels. Mean ± SE, n = 3 biological replicates. Corresponding curves obtained by switching the background gas to low O_2 are shown in Figure 3. Lines show modelled responses obtained through a combined biochemical model of light and dark reactions of C_4 photosynthesis. Model parameters are described in Note S6 and listed in Table S1, details are given in supporting notes S1 to S6.

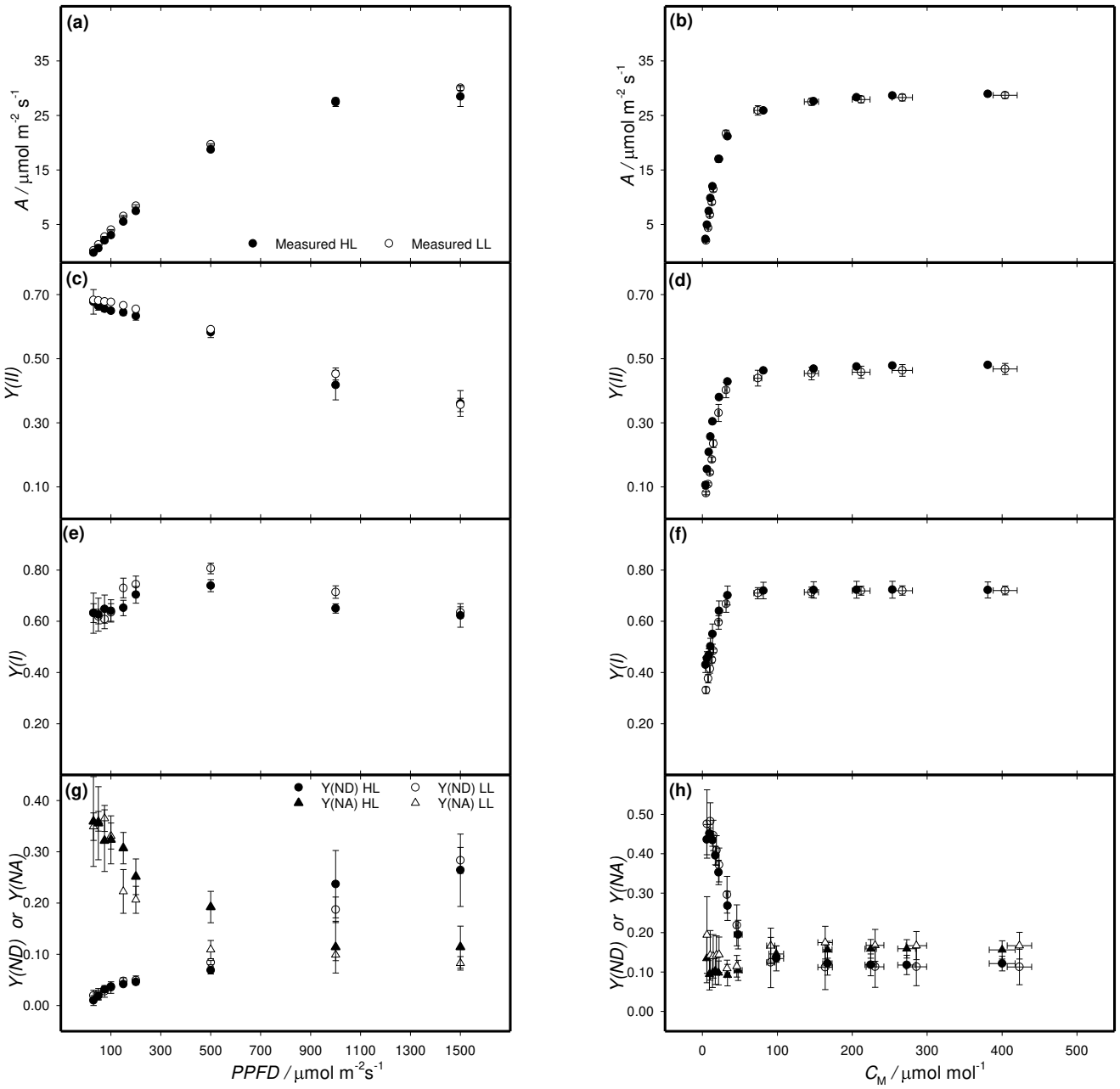

Figure 4. Measured gas–exchange and photosystems yield at 2 % O_2. Light curves measured under a reference [CO_2] of 420 µmol mol^{-1} are shown in left panels, CO_2 response curves obtained under constant irradiance of 1000 µmol m^{-2} s^{-1} are shown in right panels. Symbols show responses curves of CO_2 assimilation (**a**, **b**), quantum yield of Photosystem II (**c**, **d**), quantum yield of Photosystem I (**e**, **f**), Photosystem I donor side [*Y(ND)*] and acceptor side [*Y(NA)*] limitations (**g**, **h**) obtained for *S. viridis* grown at high light (HL, solid circles) and low light (LL, empty circles). Mean ± SE, n = 3 biological replicates. C_M, CO_2 concentration in M cells.

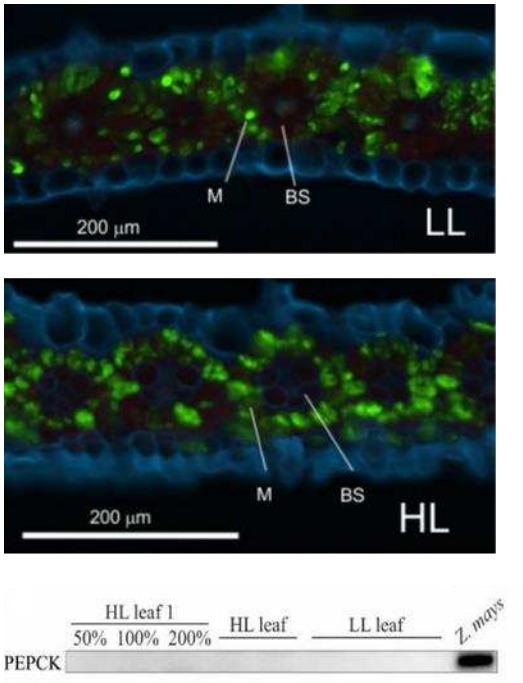

Figure 5. Protein assays for model parameterisation. Fluorescent micrographs of pyruvate ortophosphate dikinase (PPDK) localisation on the leaf cross-sections of *S. viridis* grown at low light (LL) and high light (HL). Fluorescence signals are pseudo-coloured: green – PPDK labelled with secondary antibodies conjugated with Alexa Fluor 488; blue – calcofluor white-stained cell walls. BS, bundle sheath cells; M, mesophyll cells. At the bottom, immunodetection of PEP carboxykinase (PEPCK) in whole leaf protein samples of *S. viridis* loaded on leaf area basis; *Z. mays* leaf sample was used for positive control. Three biological replicates were loaded for HL and LL plants.

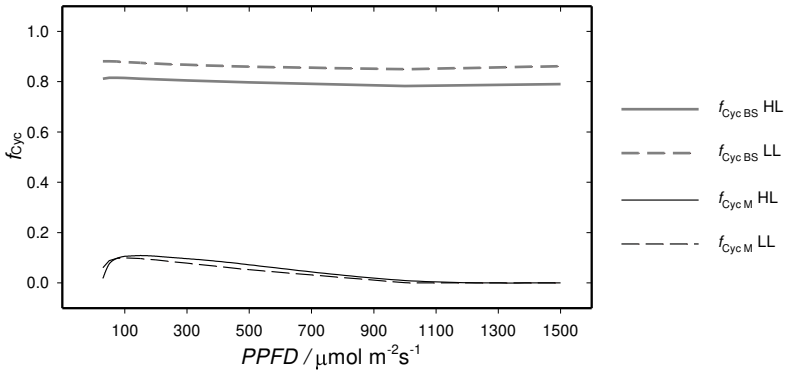

Figure 6. Responses to *PPFD* of the fitted fraction of CEF relative to total electron flow through Photosystem I (f_{Cyc}) in the M (thin black lines) or the BS (thick grey lines) of HL plants (solid) or LL plants (dashed).

References

Aoyagi, K. and Nakamoto, H. (1985) Pyruvate, Pi Dikinase in Bundle Sheath Strands as Well as in Mesophyll Cells in Maize Leaves. *Plant Physiology*, **78**, 661-664.

Bailey, K.J., Gray, J.E., Walker, R.P. and Leegood, R.C. (2007) Coordinate Regulation of Phosphoenolpyruvate Carboxylase and Phosphoenolpyruvate Carboxykinase by Light and CO2 during C4 Photosynthesis. *Plant Physiology*, **144**, 479-486.

Baker, N.R., Long, S.P. and Ort, D.R. (1988) Photosynthesis and temperature, with particular reference to effects on quantum yield. In *Plants and temperature: Society for Experimental Biology Symposium No XXXXII* (P, L.S. and I, W.F. eds): Company of biologists, pp. 347-375.

Bellasio, C. (2017) A generalised stoichiometric model of C3, C2, C2+C4, and C4 photosynthetic metabolism. *Journal of Experimental Botany*, **68**, 269-282.

Bellasio, C. (2019) A generalised dynamic model of leaf-level C3 photosynthesis combining light and dark reactions with stomatal behaviour. *Photosynthesis Research*, **141**, 99-118.

Bellasio, C., Beerling, D.J. and Griffiths, H. (2016a) Deriving C_4 photosynthetic parameters from combined gas exchange and chlorophyll fluorescence using an Excel tool: theory and practice. *Plant, Cell & Environment*, **39**, 1164-1179.

Bellasio, C., Beerling, D.J. and Griffiths, H. (2016b) An Excel tool for deriving key photosynthetic parameters from combined gas exchange and chlorophyll fluorescence: theory and practice. *Plant Cell and Environment*, **39**, 1180–1197.

Bellasio, C., Burgess, S.J., Griffiths, H. and Hibberd, J.M. (2014) A high throughput gas exchange screen for determining rates of photorespiration or regulation of C4 activity. *Journal of Experimental Botany*, **65**, 3769-3779.

Bellasio, C. and Farquhar, G.D. (2019) A leaf-level biochemical model simulating the introduction of C2 and C4 photosynthesis in C3 rice: gains, losses and metabolite fluxes. *New Phytologist*, **223**, 150-166.

Bellasio, C. and Griffiths, H. (2014a) Acclimation of C4 metabolism to low light in mature maize leaves could limit energetic losses during progressive shading in a crop canopy. *Journal of Experimental Botany*, **65**, 3725-3736.

Bellasio, C. and Griffiths, H. (2014b) Acclimation to Low Light by C4 maize: Implications for Bundle Sheath Leakiness. *Plant Cell and Environment*, **37**, 1046-1058.

Bellasio, C. and Griffiths, H. (2014c) The operation of two decarboxylases (NADPME and PEPCK), transamination and partitioning of C4 metabolic processes between mesophyll and bundle sheath cells allows light capture to be balanced for the maize C4 pathway. *Plant Physiology*, **164**, 466-480.

Bellasio, C. and Lundgren, M.R. (2016) Anatomical constraints to C4 evolution: light harvesting capacity in the bundle sheath. *New Phytologist*, **212**, 485–496.

Boesgaard, K.S., Mikkelsen, T.N., Ro-Poulsen, H. and Ibrom, A. (2013) Reduction of molecular gas diffusion through gaskets in leaf gas exchange cuvettes by leaf-mediated pores. *Plant, Cell & Environment*, **36**, 1352-1362.

Brutnell, T.P., Wang, L., Swartwood, K., Goldschmidt, A., Jackson, D., Zhu, X.-G., Kellogg, E. and Van Eck, J. (2010) Setaria viridis: a model for C4 photosynthesis. *The Plant Cell Online*, **22**, 2537-2544.

Buckley, T.N. and Adams, M.A. (2011) An analytical model of non-photorespiratory CO2 release in the light and dark in leaves of C3 species based on stoichiometric flux balance. *Plant, Cell & Environment*, **34**, 89-112.

Covshoff, S., Furbank, R.T., Leegood, R.C. and Hibberd, J.M. (2012) Leaf rolling allows quantification of mRNA abundance in mesophyll cells of sorghum. *Journal of Experimental Botany*, **64**, 807-813.

Drozak, A. and Romanowska, E. (2006) Acclimation of mesophyll and bundle sheath chloroplasts of maize to different irradiances during growth. *Biochimica et Biophysica Acta (BBA) - Bioenergetics*, **1757**, 1539-1546.

Ermakova, M., Arrivault, S., Giuliani, R., Danila, F., Alonso-Cantabrana, H., Vlad, D., Ishihara, H., Feil, R., Guenther, M., Borghi, G.L., Covshoff, S., Ludwig, M., Cousins, A.B., Langdale, J.A., Kelly, S., Lunn, J.E., Stitt, M., von Caemmerer, S. and Furbank, R.T. (2020) Installation of C4 photosynthetic pathway enzymes in rice using a single construct. *Plant Biotechnology Journal*, **doi.org/10.1111/pbi.13487**.

Ermakova, M., Bellasio, C., Fitzpatrick, D., Furbank, R., Mamedov, F. and von Caemmerer, S. (2021) Upregulation of bundle sheath electron transport capacity under limiting light in C4 Setaria viridis. *The Plant Journal*.

Ermakova, M., Lopez-Calcagno, P.E., Raines, C.A., Furbank, R.T. and von Caemmerer, S. (2019) Overexpression of the Rieske FeS protein of the Cytochrome b_6f complex increases C_4 photosynthesis in *Setaria viridis*. *Communications Biology* https://doi.org/10.1038/s42003-42019-40561-42009.

Evans, J.R., Von Caemmerer, S. and Adams, W.W., III (1991) Ecology of Photosynthesis in Sun and Shade. *Tree Physiology*, **8**, 213-213.

Evans, J.R., von Caemmerer, S., Setchell, B.A. and Hudson, G.S. (1994) The Relationship between Co2 Transfer Conductance and Leaf Anatomy in Transgenic Tobacco with a Reduced Content of Rubisco. *Australian Journal of Plant Physiology*, **21**, 475-495.

Evans, J.R., von Caemmerer, S. and Vogelmann, T.C. (2007) Balancing light capture with distributed metabolic demand during C4 photosynthesis. In *Charting new pathways to C4 rice* (J.E., S., P.L., M. and B., H. eds): IRRI International Rice Research Institute.

Farquhar, G.D. (1983) On the Nature of Carbon Isotope Discrimination in C4 Species. *Aust J Plant Physiol*, **10**, 205-226.

Furbank, R., Jenkins, C. and Hatch, M. (1990) C4 Photosynthesis: Quantum Requirement, C4 and Overcycling and Q-Cycle Involvement. *Functional Plant Biology*, **17**, 1-7.

Furbank, R.T. (2011) Evolution of the C4 photosynthetic mechanism: are there really three C4 acid decarboxylation types? *Journal of Experimental Botany*, **62**, 3103-3108.

Genty, B., Briantais, J.M. and Baker, N.R. (1989) The relationship between the quantum yield of photosynthetic electron-transport and quenching of chlorophyll fluorescence. *Biochimica Et Biophysica Acta*, **990**, 87-92.

Henderson, S.A., Von Caemmerer, S. and Farquhar, G.D. (1992) Short-Term Measurements of Carbon Isotope Discrimination in Several C4 Species. *Aust J Plant Physiol*, **19**, 263-285.

Henry, C., Watson-Lazowski, A., Oszvald, M., Griffiths, C., Paul, M.J., Furbank, R.T. and Ghannoum, O. (2019) Sugar sensing responses to low and high light in leaves of the C4 model grass Setaria viridis. *Journal of Experimental Botany*, **71**, 1039-1052.

Ishikawa, N., Takabayashi, A., Noguchi, K., Tazoe, Y., Yamamoto, H., von Caemmerer, S., Sato, F. and Endo, T. (2016) NDH-Mediated Cyclic Electron Flow Around Photosystem I is Crucial for C4 Photosynthesis. *Plant and Cell Physiology*, **57**, 2020-2028.

Ivanov, B., Asada, K., Kramer, D.M. and Edwards, G. (2005) Characterization of photosynthetic electron transport in bundle sheath cells of maize. I. Ascorbate effectively stimulates cyclic electron flow around PSI. *Planta*, **220**, 572-581.

John, C.R., Smith-Unna, R.D., Woodfield, H. and Hibberd, J.M. (2014) Evolutionary convergence of cell specific gene expression in independent lineages of C4 grasses. *Plant Physiology*.

Kanai, R. and Edwards, G.E. (1999) The biochemistry of C4 photosynthesis. In *C4 plant biology* (Sage, R.F. and Monson, R.K. eds). San Diego: Academic Press.

Klughammer, C. and Schreiber, U. (2008) Saturation Pulse method for assessment of energy conversion in PS I. *PAM Application notes*, **1**, 3.

Kramer, D.M. and Evans, J.R. (2011) The Importance of Energy Balance in Improving Photosynthetic Productivity. *Plant Physiology*, **155**, 70-78.

Kromdijk, J., Griffiths, H. and Schepers, H.E. (2010) Can the progressive increase of C4 bundle sheath leakiness at low PFD be explained by incomplete suppression of photorespiration? *Plant Cell and Environment*, **33**, 1935-1948.

Kromdijk, J., Ubierna, N., Cousins, A.B. and Griffiths, H. (2014) Bundle-sheath leakiness in C4 photosynthesis: a careful balancing act between CO2 concentration and assimilation. *Journal of Experimental Botany*, **65**, 3443-3457.

Li, P. and Brutnell, T.P. (2011) Setaria viridis and Setaria italica, model genetic systems for the Panicoid grasses. *Journal of Experimental Botany*, **62**, 3031-3037.

Li, X.-P., Gilmore, A.M., Caffarri, S., Bassi, R., Golan, T., Kramer, D. and Niyogi, K.K. (2004) Regulation of Photosynthetic Light Harvesting Involves Intrathylakoid Lumen pH Sensing by the PsbS Protein. *Journal of Biological Chemistry*, **279**, 22866-22874.

Long, S.P. (1993) The significance of light-limited photosynthesis to crop canopy carbon gain and productivity - a theoretical analysis. In *Photosynthesis: Photoreactions to Plant Productivity* (Abrol, Y.P., Mohanty, P. and Govindjee eds). New Delhi: Oxford & IBH publishing, pp. 547 - 560.

Maai, E., Nishimura, K., Takisawa, R. and Nakazaki, T. (2020a) Diurnal changes in chloroplast positioning and photosynthetic traits of C4 grass finger millet. *Plant Production Science*, 1-13.

Maai, E., Nishimura, K., Takisawa, R. and Nakazaki, T. (2020b) Light stress-induced chloroplast movement and midday depression of photosynthesis in sorghum leaves. *Plant Production Science*, **23**, 172-181.

Majeran, W. and van Wijk, K.J. (2009) Cell-type-specific differentiation of chloroplasts in C4 plants. *Trends in Plant Science*, **14**, 100-109.

Osmond, C. (1974) Carbon reduction and photosystem II deficiency in leaves of C4 plants. *Aust J Plant Physiol*, **1**, 41-50.

Pengelly, J.J.L., Sirault, X.R.R., Tazoe, Y., Evans, J.R., Furbank, R.T. and von Caemmerer, S. (2010) Growth of the C4 dicot Flaveria bidentis: photosynthetic acclimation to low light through shifts in leaf anatomy and biochemistry. *Journal of Experimental Botany*, **61**, 4109-4122.

Peterson, R.B., Schultes, N.P., McHale, N.A. and Zelitch, I. (2016) Evidence for a Role for NAD(P)H Dehydrogenase in Concentration of CO₂ in the Bundle Sheath Cell of <em>Zea mays</em&gt. *Plant Physiology*, **171**, 125.

Porra, R.J., Thompson, W.A. and Kriedemann, P.E. (1989) Determination of accurate extinction coefficients and simultaneous equations for assaying chlorophylls a and b extracted with four different solvents: verification of the concentration of chlorophyll standards by atomic absorption spectroscopy. *Biochimica et Biophysica Acta (BBA) - Bioenergetics*, **975**, 384-394.

Rogowski, P., Wasilewska-Dębowska, W., Krupnik, T., Drożak, A., Zienkiewicz, M., Krysiak, M. and Romanowska, E. (2019) Photosynthesis and organization of maize mesophyll and bundle sheath thylakoids of plants grown in various light intensities. *Environmental and Experimental Botany*, **162**, 72-86.

Romanowska, E., Drożak, A., Pokorska, B., Shiell, B.J. and Michalski, W.P. (2006) Organization and activity of photosystems in the mesophyll and bundle sheath chloroplasts of maize. *Journal of Plant Physiology*, **163**, 607-618.

Sage, R.F. (2017) A portrait of the C4 photosynthetic family on the 50th anniversary of its discovery: species number, evolutionary lineages, and Hall of Fame. *Journal of experimental botany*, **68**, e11-e28.

Sage, R.F., Christin, P.-A. and Edwards, E.J. (2011) The C4 plant lineages of planet Earth. *Journal of Experimental Botany*, **62**, 3155-3169.

Sales, C.R.G., Ribeiro, R.V., Hayashi, A.H., Marchiori, P.E.R., Silva, K.I., Martins, M.O., Silveira, J.A.G., Silveira, N.M. and Machado, E.C. (2018) Flexibility of C4 decarboxylation and photosynthetic plasticity in sugarcane plants under shading. *Environmental and Experimental Botany*, **149**, 34-42.

Schlüter, U. and Weber, A.P.M. (2020) Regulation and Evolution of C4 Photosynthesis. *Annual Review of Plant Biology*, **71**, null.

Sharwood, R.E., Sonawane, B.V. and Ghannoum, O. (2014) Photosynthetic flexibility in maize exposed to salinity and shade. *Journal of experimental botany*, **65**, 3715-3724.

Sonawane, B.V., Sharwood, R.E., Whitney, S. and Ghannoum, O. (2018) Shade Compromises the Photosynthetic Efficiency of NADP-ME less than PEP-CK and NAD-ME C4 Grasses. *Journal of Experimental Botany*, **69**, 3053–3068.

Spilatro, S.R. and Preiss, J. (1987) Regulation of starch synthesis in the bundle sheath and mesophyll of Zea mays L. Intercellular compartmentalization of enzymes of starch metabolism and the properties of the ADPglucose pyrophosphorylases. *Plant Physiology*, **83**, 621-627.

Takabayashi, A., Kishine, M., Asada, K., Endo, T. and Sato, F. (2005) Differential use of two cyclic electron flows around photosystem I for driving CO2-concentration mechanism in C4 photosynthesis. *Proceedings of the National Academy of Sciences of the United States of America*, **102**, 16898-16903.

Takagi, D., Hashiguchi, M., Sejima, T., Makino, A. and Miyake, C.J.P.R. (2016) Photorespiration provides the chance of cyclic electron flow to operate for the redox-regulation of P700 in photosynthetic electron transport system of sunflower leaves. **129**, 279-290.

Terashima, I., Fujita, T., Inoue, T., Chow, W.S. and Oguchi, R. (2009) Green Light Drives Leaf Photosynthesis More Efficiently than Red Light in Strong White Light: Revisiting the Enigmatic Question of Why Leaves are Green. *Plant and Cell Physiology*, **50**, 684-697.

Ubierna, N., Gandin, A., Boyd, R.A. and Cousins, A.B. (2017) Temperature response of mesophyll conductance in three C4 species calculated with two methods: 18O discrimination and in vitro Vpmax. *New Phytologist*, **214**, 66–80.

Ubierna, N., Sun, W., Kramer, D.M. and Cousins, A.B. (2013) The Efficiency Of C4 Photosynthesis Under Low Light Conditions In Zea mays, Miscanthus X giganteus And Flaveria bidentis. *Plant, Cell & Environment*, **36**, 365-381.

von Caemmerer, S. (2000) *Biochemical models of leaf Photosynthesis* Collingwood: CSIRO Publishing.

von Caemmerer, S., Evans, J., Cousins, A., Badger, M. and Furbank, R.T. (2008) C 4 photosynthesis and CO 2 diffusion. In *Charting new pathways to C4 rice*: World Scientific, pp. 95-115.

von Caemmerer, S. and Furbank, R.T. (1999) Modelling C4 photosynthesis. In *The biology of C4 Photosynthesis* (Sage, R.F. and Monson, R.K. eds). London: Academic Press, pp. 173-211.

von Caemmerer, S. and Furbank, R.T. (2003) The C4 pathway: an efficient CO2 pump. *Photosynthesis Research*, **77**, 191-207.

Ward, D.A. and Woolhouse, H.W. (1986) Comparative effects of light during growth on the photosynthetic properties of NADP-ME type C4 grasses from open and shaded habitats. I. Gas exchange, leaf anatomy and ultrastructure*. *Plant, Cell & Environment*, **9**, 261-270.

Weber, A.P.M. and von Caemmerer, S. (2010) Plastid transport and metabolism of C3 and C4 plants — comparative analysis and possible biotechnological exploitation. *Current Opinion in Plant Biology*, **13**, 256-264.

Wingler, A., Walker, R.P., Chen, Z.H. and Leegood, R.C. (1999) Phosphoenolpyruvate carboxykinase is involved in the decarboxylation of aspartate in the bundle sheath of maize. *Plant Physiology*, **120**, 539-545.

Yamada, M., Kawasaki, M., Sugiyama, T., Miyake, H. and Taniguchi, M. (2009) Differential Positioning of C4 Mesophyll and Bundle Sheath Chloroplasts: Aggregative Movement of C4 Mesophyll Chloroplasts in Response to Environmental Stresses. *Plant and Cell Physiology*, **50**, 1736-1749.

Yin, X.Y. and Struik, P.C. (2012) Mathematical review of the energy transduction stoichiometries of C4 leaf photosynthesis under limiting light. *Plant Cell and Environment*, **35**, 1299-1312.

Yin, X.Y., Sun, Z.P., Struik, P.C., Van der Putten, P.E.L., Van Ieperen, W. and Harbinson, J. (2011) Using a biochemical C4 photosynthesis model and combined gas exchange and chlorophyll fluorescence measurements to estimate bundle-sheath conductance of maize leaves differing in age and nitrogen content. *Plant Cell and Environment*, **34**, 2183-2199.